New Phytologist Supporting Information:

Horizontal chromosome transfer and convergent evolution drive diversification in *Fusarium oxysporum* f. sp. *fragariae*.

Peter M. Henry, Dominique D.A. Pincot, Bradley Jenner, Celia Borrero, Manuel Aviles, Myeong-Hyeon Nam, Lynn Epstein, Steven J. Knapp, Thomas R. Gordon

Article Acceptance Date: Dec. 2, 2020

Fig. S1. Pictures corresponding to disease ratings for wilt- and yellows-*fragariae*. The upper panel has top-view and side-view photos of plants corresponding to each symptom rating on the 1 to 5 ordinal scale used to rate plants inoculated with wilt-*fragariae* isolates. For wilt-*fragariae* isolates, (which did not cause chlorosis), plants were rated on a 1-5 scale corresponding to the following symptoms: 1 = no symptoms, 2 = 0-25% of leaves wilted, 3 = 25-50% of leaves wilted, 4 = more than 50% of leaves wilted, but at least one leaf has turgor, and 5 = dead (all leaves wilted/brown).

The bottom panel has photos from plants inoculated with yellows-*fragariae* isolates corresponding to the 1 to 5 ordinal disease severity rating scale. For yellows-fragariae isolates, (which caused chlorosis), ordinal ratings were: 1 = no symptoms, 2 = mild stunting, marginal chlorosis, 3 = youngest leaves fully chlorotic, 4 = outer leaves chlorotic, some wilting observed, and 5 = dead (all leaves were brown).

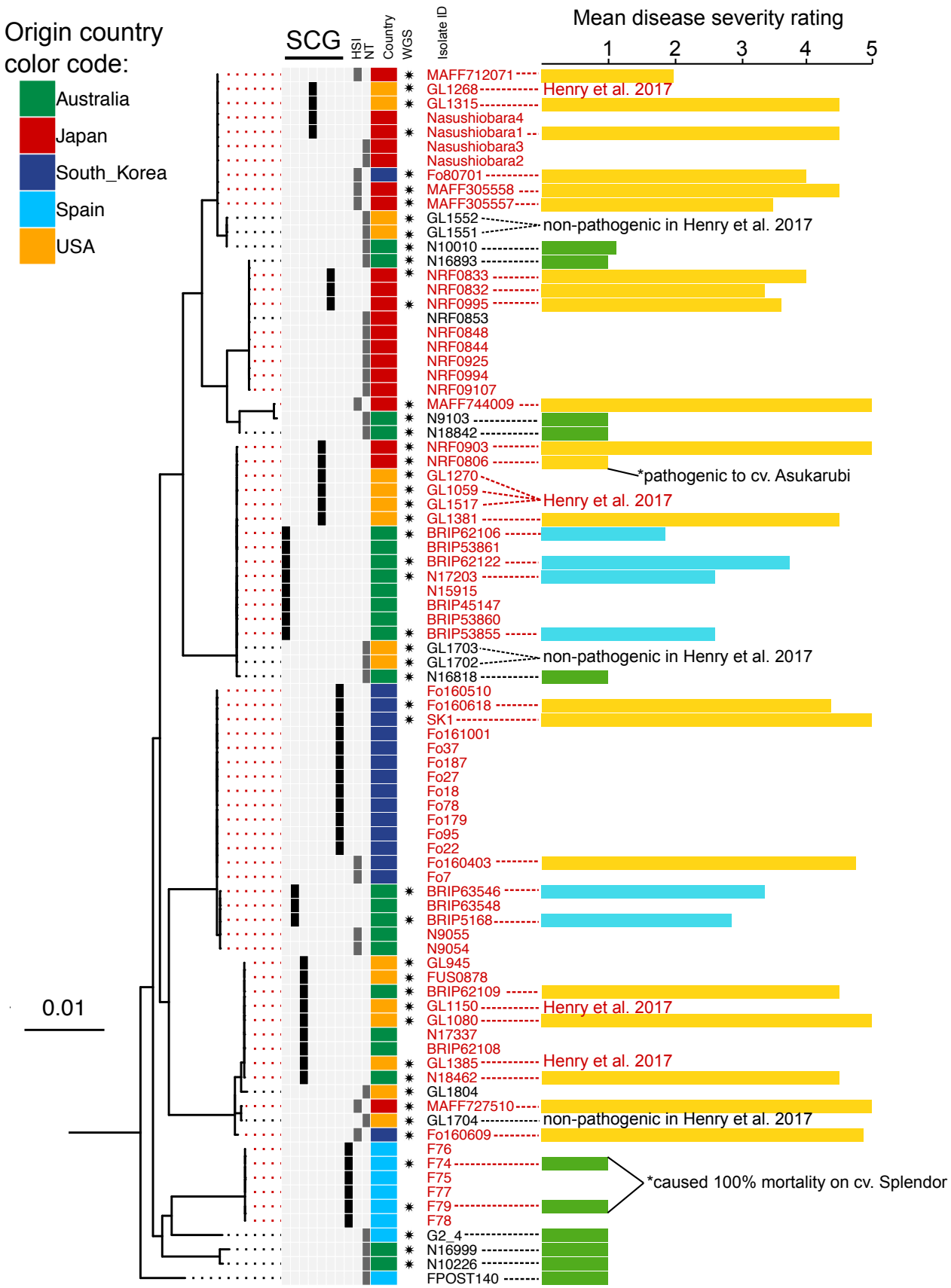
Origin country color code:
Australia
Japan
South_Korea
Spain
USA
SCG
HSI NT
Country
WGS
Isolate ID
Mean disease severity rating
1
2
3
4
5
MAFF712071
GL1268
GL1315
Nasushiobara4
Nasushiobara1
Nasushiobara3
Nasushiobara2
Fo80701
MAFF305558
MAFF305557
GL1552
GL1551
N10010
N16893
NRF0833
NRF0832
NRF0995
NRF0853
NRF0848
NRF0844
NRF0925
NRF0994
NRF09107
MAFF744009
N9103
N18842
NRF0903
NRF0806
GL1270
GL1059
GL1517
GL1381
BRIP62106
BRIP53861
BRIP62122
N17203
N15915
BRIP45147
BRIP53860
BRIP53855
GL1703
GL1702
N16818
Fo160510
Fo160618
SK1
Fo161001
Fo37
Fo187
Fo27
Fo18
Fo78
Fo179
Fo95
Fo22
Fo160403
Fo7
BRIP63546
BRIP63548
BRIP5168
N9055
N9054
GL945
FUS0878
BRIP62109
GL1150
GL1080
N17337
BRIP62108
GL1385
N18462
GL1804
MAFF727510
GL1704
Fo160609
F76
F74
F75
F77
F79
F78
G2_4
N16999
N10226
FPOST140
Henry et al. 2017
non-pathogenic in Henry et al. 2017
*pathogenic to cv. Asukarubi
Henry et al. 2017
non-pathogenic in Henry et al. 2017
Henry et al. 2017
Henry et al. 2017
non-pathogenic in Henry et al. 2017
*caused 100% mortality on cv. Splendor
0.01

Fig. S2. Overview of isolates used in this study. The phylogenetic tree is the output of a maximum likelihood analysis of aligned and concatenated intergenic spacer (IGS) and elongation factor 1-alpha (EF-1α) sequences. Somatic compatibility groups are denoted by black boxes in the same column. Dark grey bars indicate the isolate is heterokaryon self-incompatible ("HSI") or that somatic compatibility could not be tested for this study ("NT"). Colored boxes indicate the country of origin. An asterisk to the left of the isolate ID indicates the whole genome was sequenced ("WGS") for the corresponding isolate. Isolates characterized as *forma specialis fragariae* have IDs colored in a red font; isolates with black font IDs are not pathogenic to strawberry. The mean pathogenicity rating on cultivar Sweet Ann at 8 weeks post inoculation is depicted for each isolate to the left of the isolate ID where 1 = healthy (non-pathogenic) and 5 = dead (highly virulent). The color of the bar indicating the mean pathogenicity corresponds to the symptom group: yellow = yellows-*fragariae*, blue = wilt-*fragariae*, and green = non-pathogenic. Citations are provided for isolates whose pathogenicity phenotype was determined in other publications.

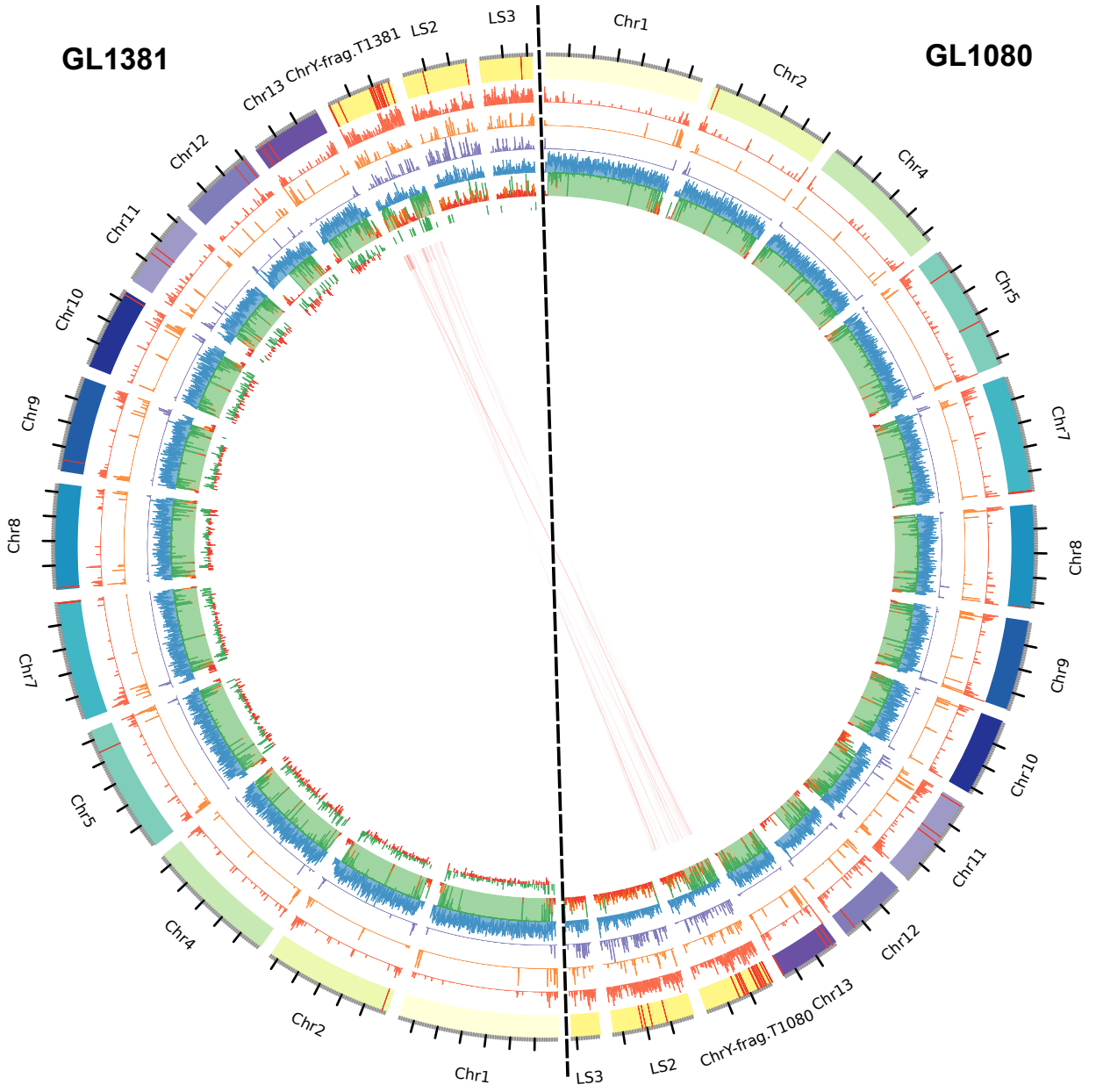

Fig. S3. Whole genome comparison of GL1381 (left) and GL1080 (right) reference assemblies. Core chromosome ideograms (Chr) are color coded and all accessory chromosomes have a yellow ideogram. Red lines through the ideogram indicate the location of miniature *impala* transposons. Annotation tracks depict the proportion of each 10 kbp window with coverage by: DNA transposons (red), LTR transposons (orange), LINEs (purple), or predicted genes (blue). Inside the blue histogram (predicted genes) is a histogram indicating the proportion of 10 kbp windows with coverage from all 27 yellows-*fragariae* isolates. This histogram is color-coded based on the proportion with coverage: green ≥ 0.66, 0.6 > orange ≥ 0.34, red < 0.33. For GL1381, the position and log-fold change of genes that were differentially expressed *in planta* are depicted inside the coverage track. Up-regulated genes are green, down-regulated genes are red, and the scale ranges from -10 to 14 log-fold change. Links between chr$^{Y\text{-frag.T1080}}$

and chr$^{Y\text{-}frag.T1381}$ indicate the positions of homologous genes that are conserved in yellows-*fragariae* on these two chromosomes.

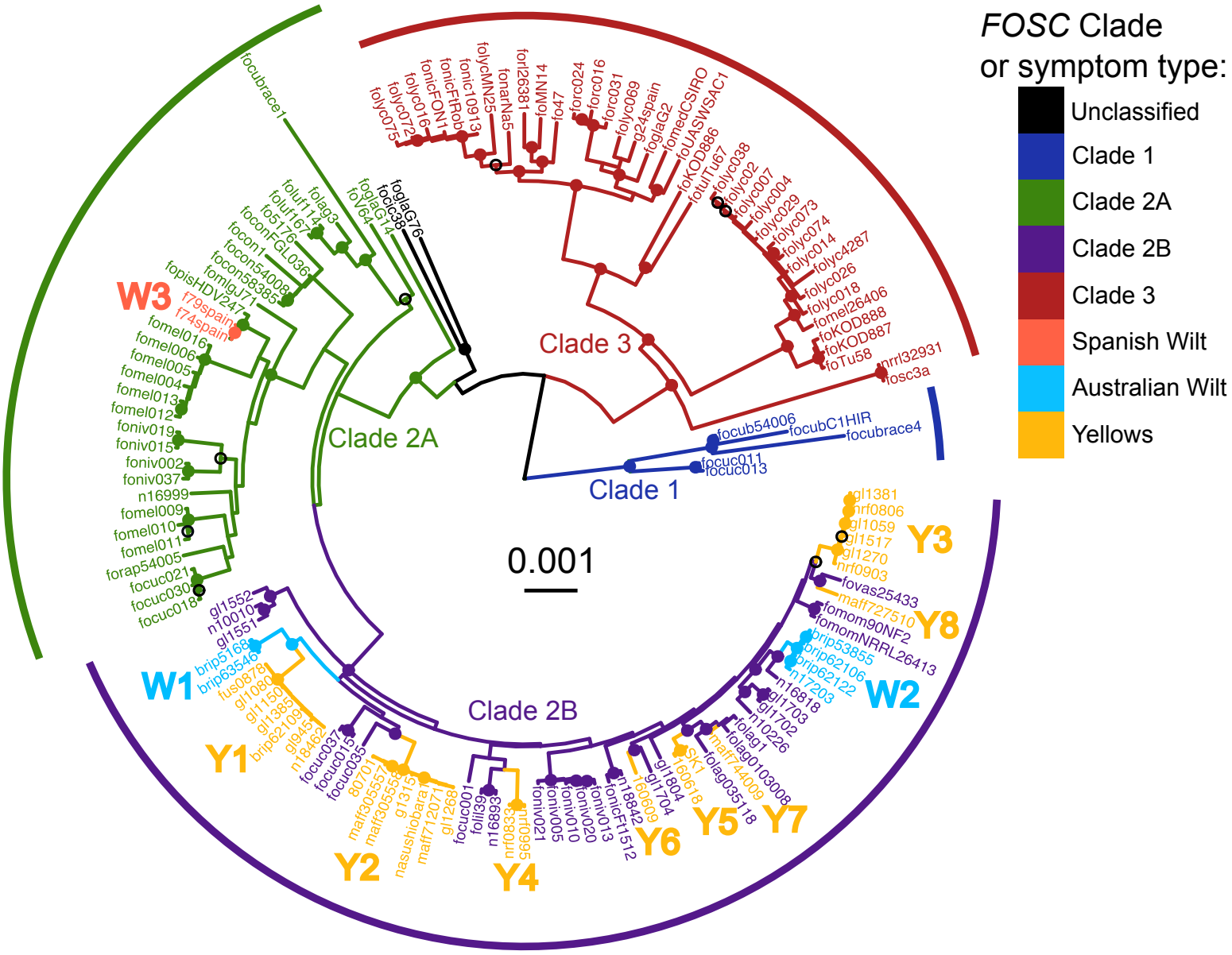

Fig S4. Core genome phylogeny of the *Fusarium oxysporum* species complex with isolate labels. Single copy orthologous genes (n=2,718) from 139 *F. oxysporum* genomes were aligned by MUSCLE and concatenated into a single, ~5.5 Mbp alignment. Maximum likelihood (ML) phylogenetic comparisons were conducted by RAxML using the general time reversible model with gamma correction and 1,000 bootstrap replicates. Branches are color-coded by *Fusarium oxysporum* f. sp. *fragariae* symptom group (Spanish wilt-*fragariae*, Australian wilt-*fragariae*, and yellows-*fragariae*) and by core genome phylogenetic clades. Nodes with a filled circle have bootstrap support >90%, a black open circle indicates bootstrap support > 70%. Monophyletic groups of yellows- and *wilt-fragariae* are annotated with Y1-Y8 and W1-W3, respectively.

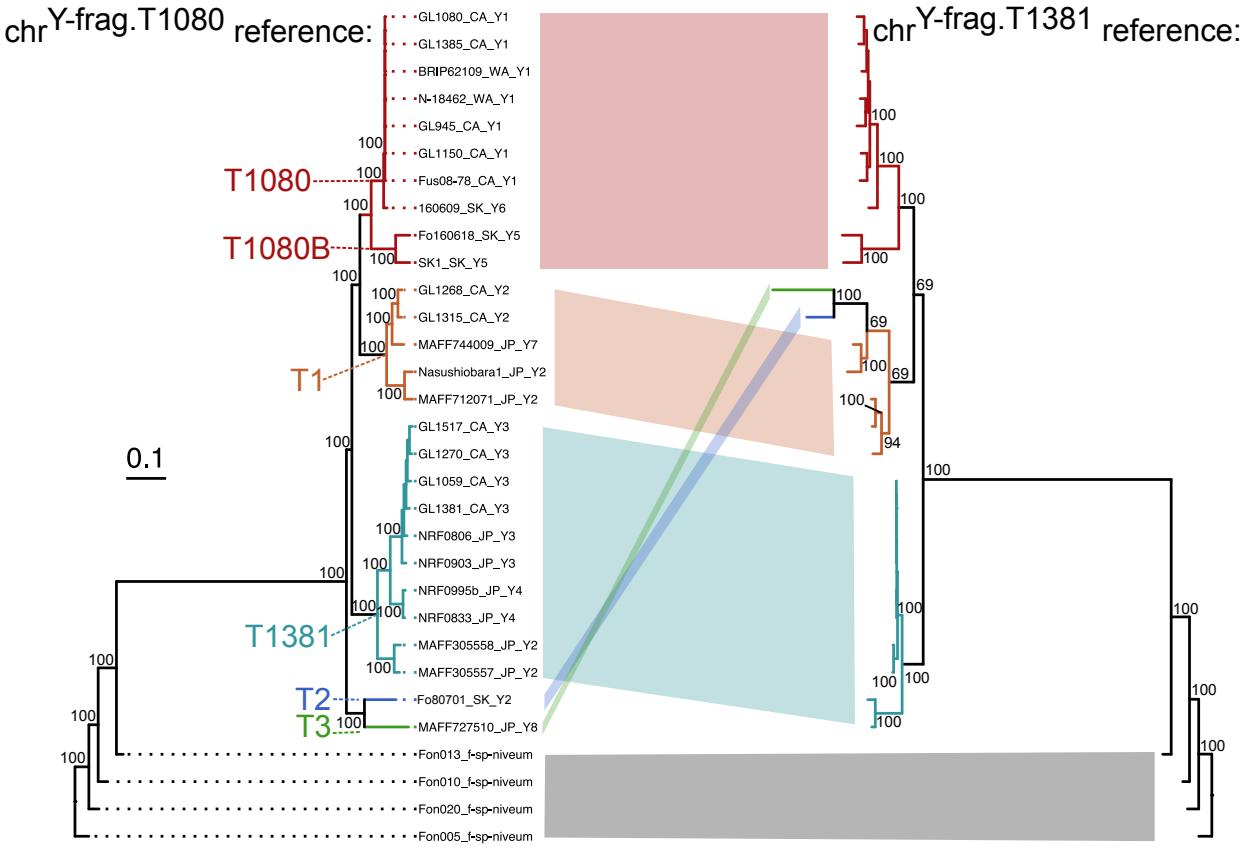

Fig. S5. Comparison of the phylogeny inferred from chr$^{Y\text{-}frag.T1080}$ and chr$^{Y\text{-}frag.T1381}$. Single nucleotide polymorphisms (SNPs) were called by freebayes (version 1.3.1) on chr$^{Y\text{-}frag.T1080}$ and chr$^{Y\text{-}frag.T1381}$. Genotype calls from SNPs in conserved regions of chr$^{Y\text{-}frag.T1080}$ and chr$^{Y\text{-}frag.T1381}$ (n = 18,122 and n = 18,421 SNPs, respectively) were concatenated and the maximum likelihood phylogeny inferred by RAxML with correction for ascertainment bias. Bootstrap values are calculated from 1,000 replicates and indicated next to their corresponding node. The chr$^{Y\text{-}frag}$ type (T1080, T1080B, T1381, T1, T2, and T3) is color coded and indicated adjacent to its corresponding clade. Colored blocks between phylograms indicate identical topology.

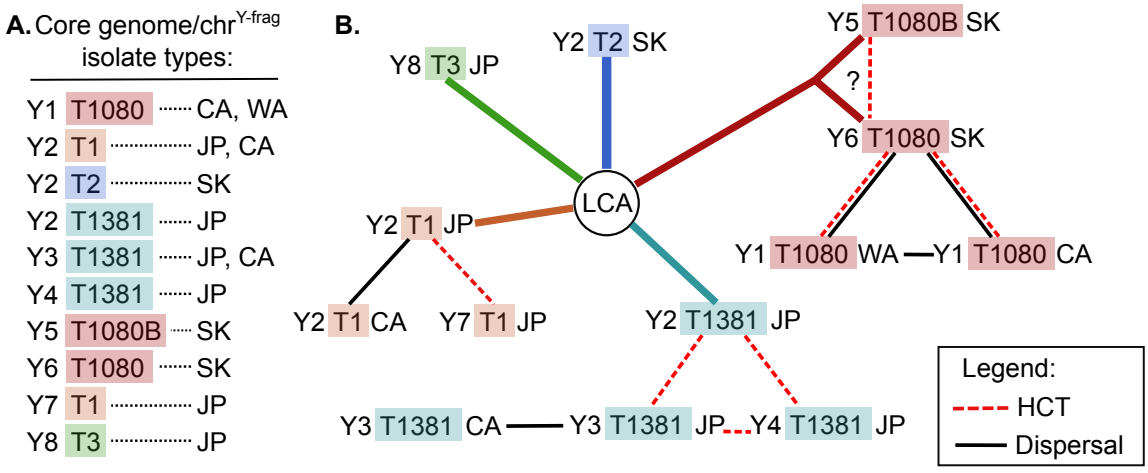

Fig. S6. Predicted events of horizontal chromosome transfer (HCT) and dispersal of core and chr$^{Y\text{-}frag}$ genotypes. **A.** An inventory of all combinations of monophyletic clades (Y1-Y8) and chr$^{Y\text{-}frag}$ types. The countries/state from which they were recovered is indicated on the right; geographic origin codes are as follows: CA = California, JP = Japan, SK = South Korea, and WA = Western Australia. **B.** The five primary chr$^{Y\text{-}frag}$ types are connected to the last common ancestor ("LCA") by colored lines. Dashed red lines connect pathogen genotypes between which HCT appears to have occurred. It is not clear if T1080B and T1080 in Y5 and Y6 diverged from the last core genome ancestor or was transferred in the past, so both possibilities are shown with an "?" in the middle. Solid black lines indicate dispersal between countries, presumably on vegetatively propagated plants. Evidence for dispersal comes from recovering the same core genome/chr$^{Y\text{-}frag}$ genotypic combination from multiple countries.

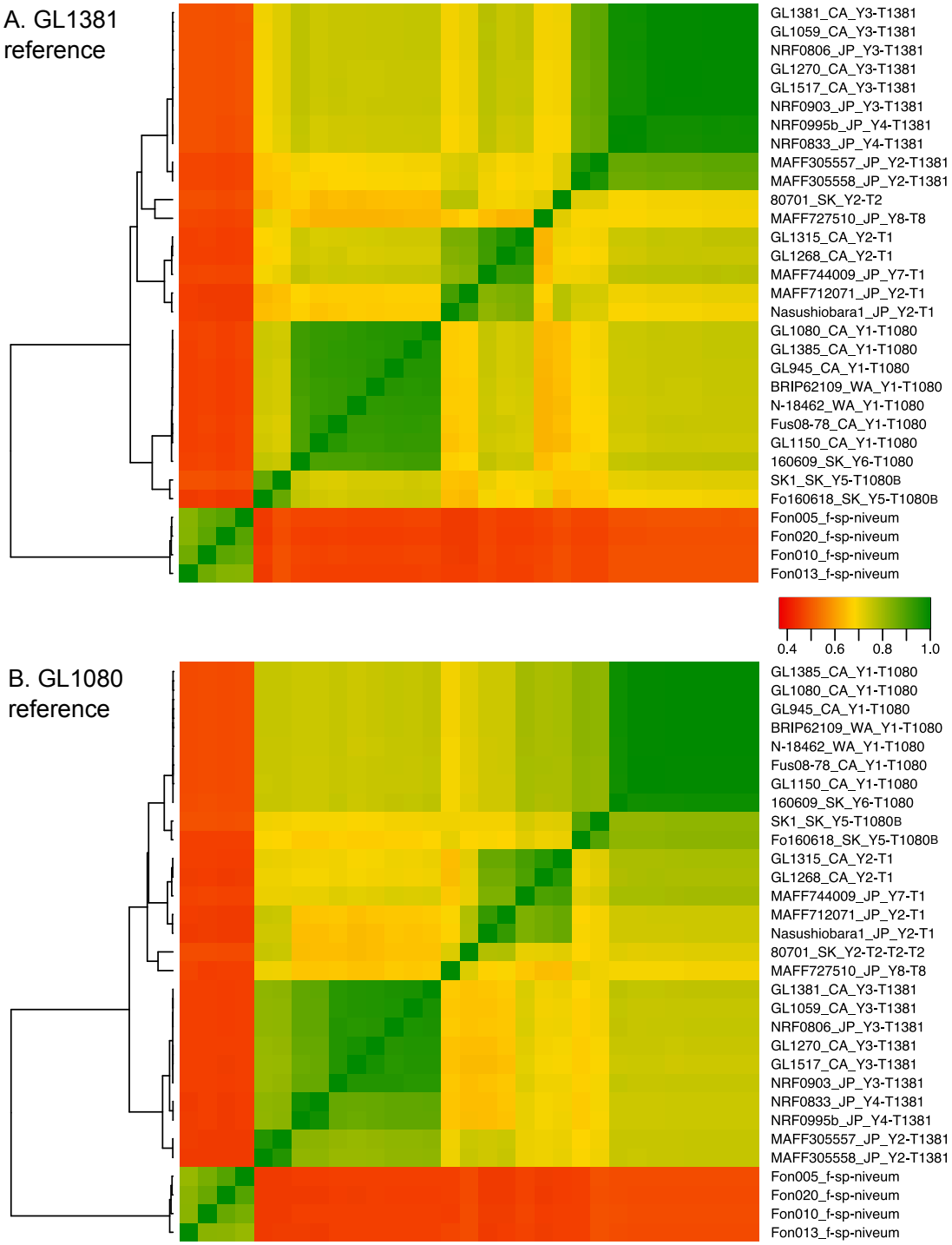

Fig. S7. Distance matrices based on the proportion of identical genotypes at single nucleotide polymorphic sites (SNPs) on A) chr$^{Y\text{-}frag.T1381}$ and B) chr$^{Y\text{-}frag.T1080}$. Freebayes was used to call variants on chr$^{Y\text{-}frag.T1080}$ and chr$^{Y\text{-}frag.T1381}$ from aligned, quality-filtered Illumina reads. Variants were filtered to retain only those present in regions with coverage for all yellows-*fragariae* isolates by bedtools 'intersect'. Pairwise isolate sequence similarity was calculated by dividing the proportion of identical alleles at variant sites by the total number of SNPs. The monophyletic yellows-*fragariae* clades

(Y1-Y8) and chr$^{Y\text{-}frag}$ type (T1, T2, T3, T1080, T1080B, and T1381) are annotated to the right of the isolate IDs. **A.** GL1381 was used as the reference isolate (n = 18,421 total SNPs). **B.** GL1080 was the reference isolate (n = 18,122 total SNPs).

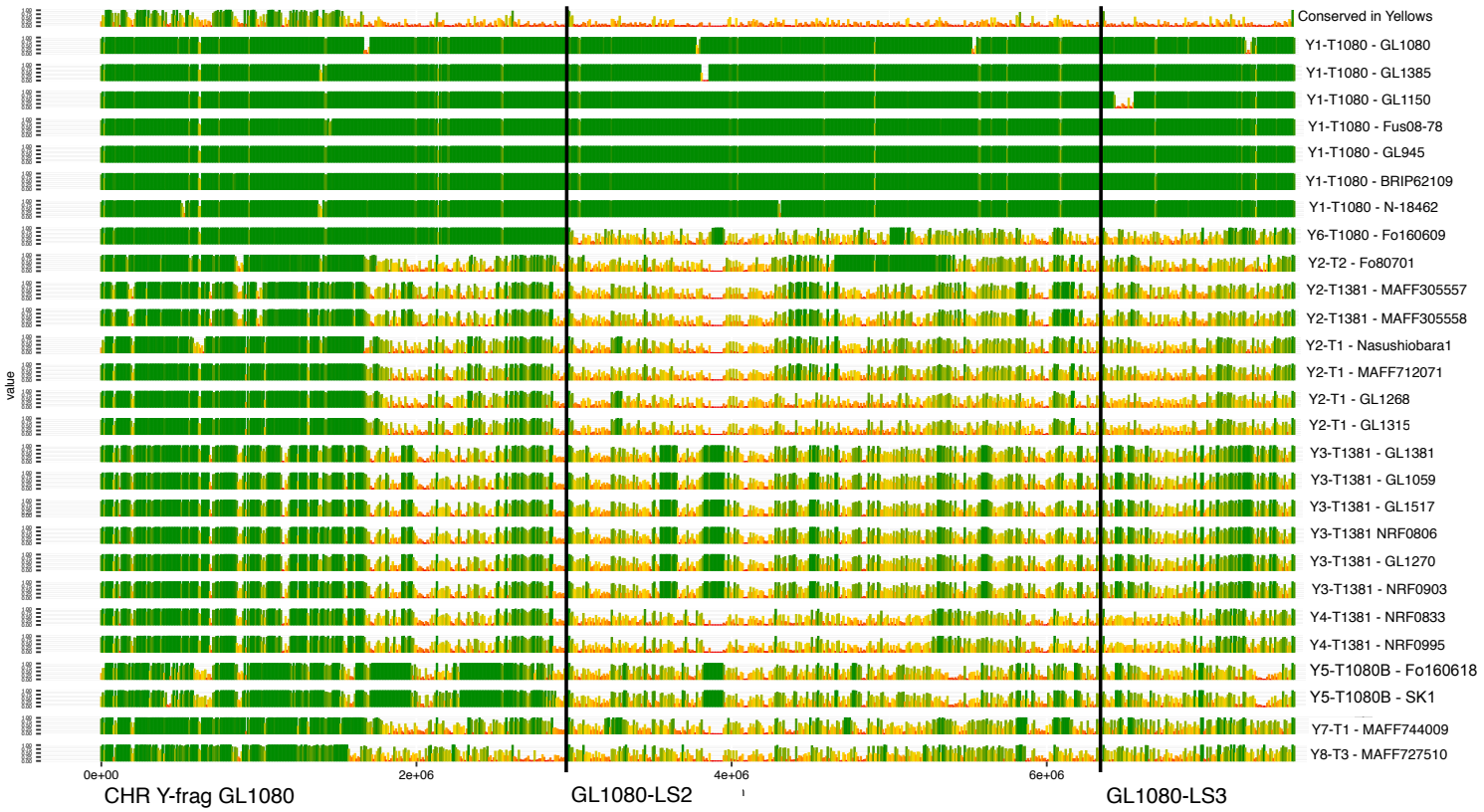

Fig. S8. Coverage of GL1080 accessory chromosomes ($chr^{Y\text{-}frag.T1080}$, lineage-specific #2 (LS2), and lineage-specific #3 (LS3)) by short, high-fidelity reads from yellows-*fragariae* isolates. Each row corresponds to a different yellows-*fragariae* isolate, which are labeled by their monophyletic group ID (Y1-Y8), $chr^{Y\text{-}frag}$ type (T1, T2, T3, T1080, T1080B, and T1381), and isolate ID on the right side of the graph. The proportion of bases per 10 kbp window (columns) that have coverage for the indicated isolate is indicated by the height and color of the bar; green is greater than 0.66, yellow is between 0.66-0.33, and red is less than 0.33. The top row depicts coverage of bases that are conserved among all yellows-*fragariae* isolates (i.e. “conserved in yellows”). The black vertical lines indicate the start/end position of each chromosome.

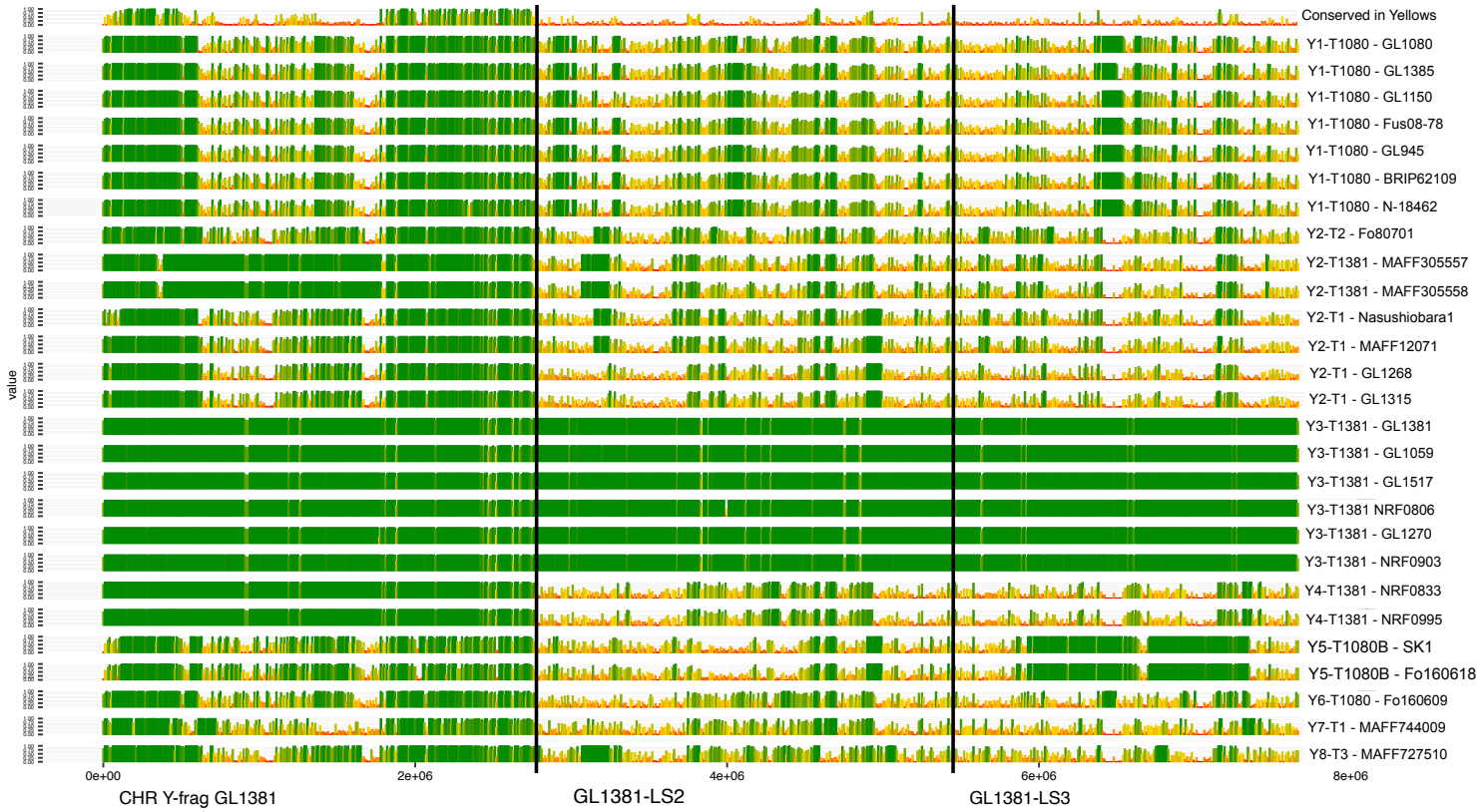

Fig. S9. Coverage of GL1381 accessory chromosomes ($chr^{Y\text{-}frag.T1381}$, lineage-specific #2 (LS2), and lineage-specific #3 (LS3)) by short, high-fidelity reads from yellows-*fragariae* isolates Each row corresponds to a different yellows-*fragariae* isolate, which are labeled by their monophyletic group ID (Y1-Y8), $chr^{Y\text{-}frag}$ type (T1, T2, T3, T1080, T1080B, and T1381), and isolate ID on the right side of the graph. The proportion of bases per 10 kbp window (columns) that have coverage for the indicated isolate is indicated by the height and color of the bar; green is greater than 0.66, yellow is between 0.66-0.33, and red is less than 0.33. The top row depicts coverage of bases that are conserved among all yellows-*fragariae* isolates (i.e. “conserved in yellows”). The black vertical lines indicate the start/end position of each chromosome.

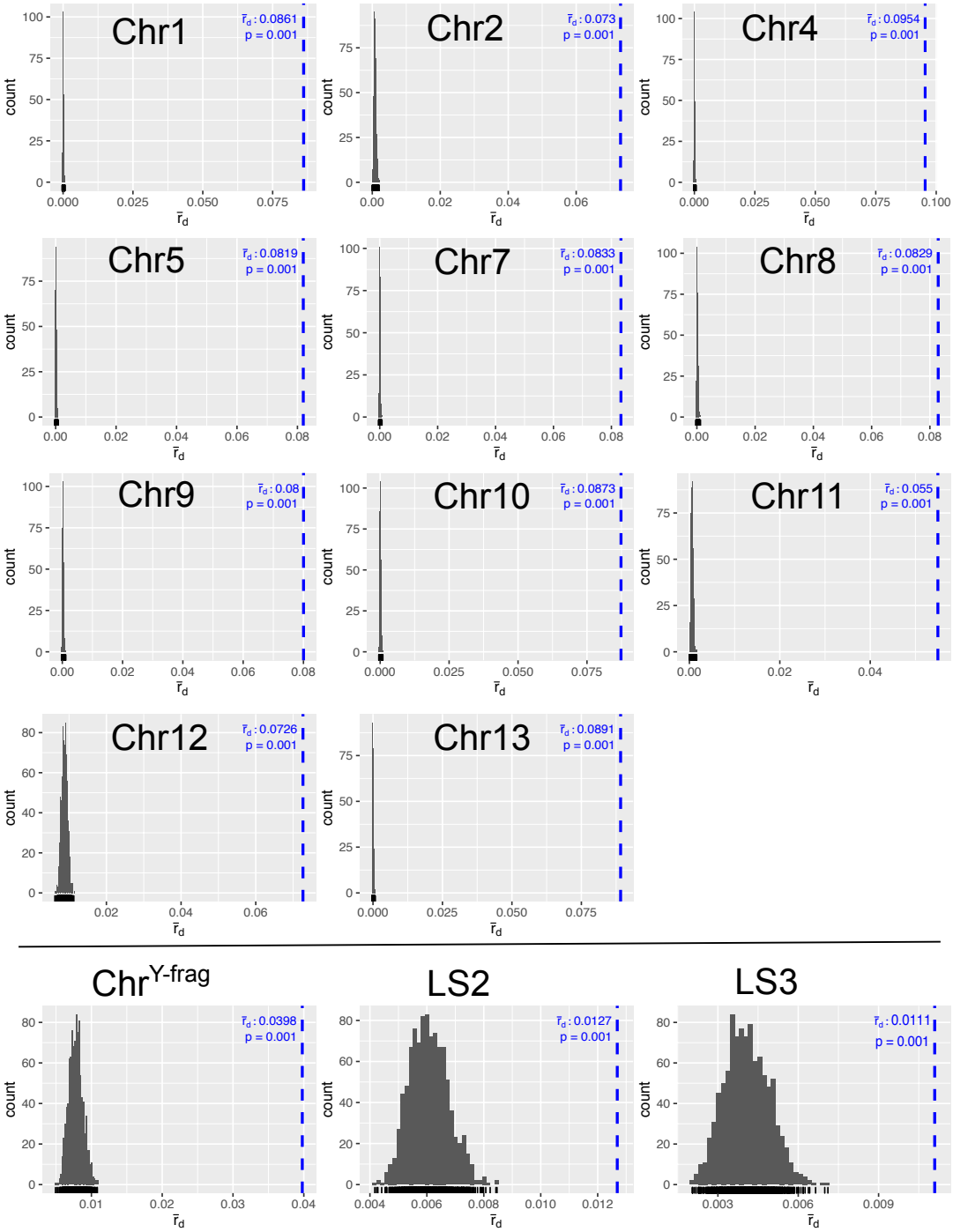

Fig S10. Index of association for variants on core chromosomes from a clone-corrected yellows-*fragariae* population. Variants were called by freebayes (version 1.3.1) from 11 yellows-*fragariae* genotypes representing each clonal lineage within the eight monophyletic clades. The output of freebayes was filtered by vcftools for quality (minQ > 30), read depth (minDP >10) and minor allele count (mac > 3), and randomly resampled with vcflib 'vcfrandomsample' to a rate of 0.05. The average proportion of SNPs to total chromosome length was 672. Linkage disequilibrium was assessed by the R package 'poppr' function 'ia()' with 999 permutations. All chromosomes exhibited strong signatures of clonality (i.e. linkage disequilibrium), with $P = 0.001$ in all analyses.

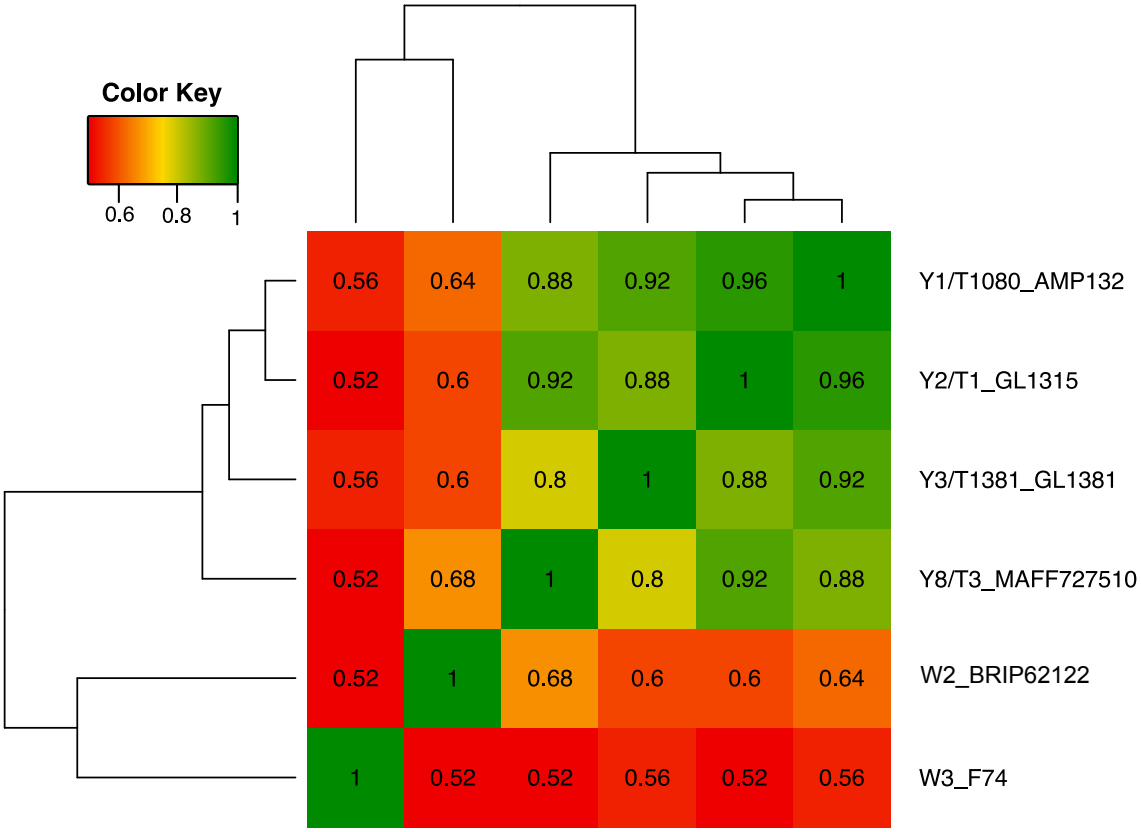

Fig. S11. The proportion of identical disease phenotypes (resistant or susceptible) between six isolates of *Fusarium oxysporum* f. sp. *fragariae*. For each combination of isolate and strawberry accession, the phenotype was considered "susceptible" if the least-squares mean was greater than or equal to 2.5, and "resistant" if the value was less than 2.5 (based on Fig. 3B). Shown are the proportion of strawberry accessions (n = 25 total) with the same phenotype (resistant or susceptible) for each pairwise combination of isolates. Disease severity was rated on a 1 to 5 ordinal scale, where 1 = asymptomatic and 5 = dead (Fig. S2).

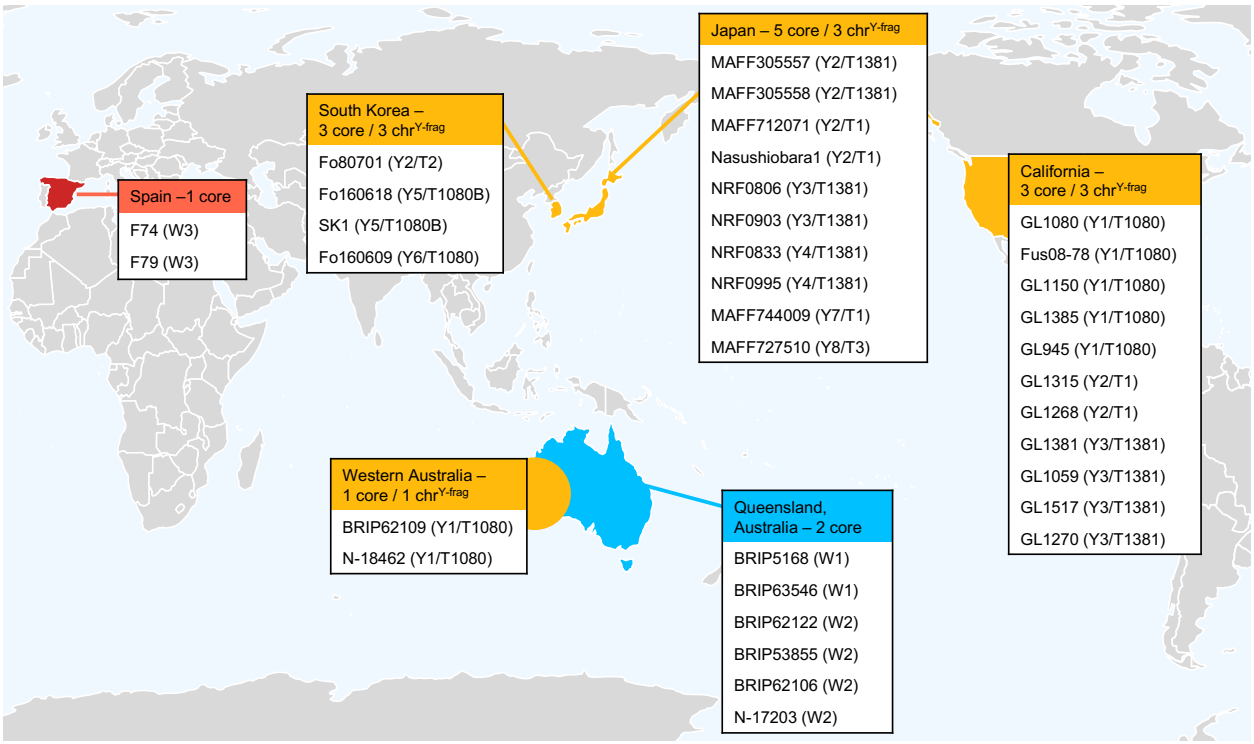

Fig. S12. Map of isolates characterized phenotypically and with whole genome sequencing for this study. The core genome clade ID (Y1-Y8 and W1-W3) are indicated parenthetically after each isolate ID. The chr$^{Y\text{-}frag}$ type is also indicated after a "/" for yellows-fragariae isolates.

Table S1. Summary of isolates characterized in this study.

Country:[a]	Not pathogenic to strawberry[b]	f. sp. *fragariae*[c]	Total # Isolates[d]
Australia	7 (6)	17 (8)	24 (14)
Japan	1 (0)	19 (10)	20 (10)
South Korea	0 (0)	16 (4)	16 (4)
Spain	2 (1)	6 (2)	8 (3)
United States (California)	6 (6)	11 (11)	17 (17)
Total	16 (13)	69 (35)	85 (48)

[a] Country of origin for isolates characterized in this study.
[b] The number of isolates that were not pathogenic to strawberry followed by the number of non-pathogens that were whole genome sequenced (in parentheses).
[c] The number of f. sp. *fragariae* isolates followed by the number of f. sp. *fragariae* isolates that were whole genome sequenced (in parentheses).
[d] The total number of isolates followed by the number that were whole genome sequenced.

Table S2. Assembly stats for scaffolded GL1080 and GL1381 genomes.

	GL1381	GL1080
Scaffold #:	33	38
Contig #:	60	63
Scaffold sequence total (bp):	56,962,690	55,751,422
Contig sequence total (bp):	56,959,990	55,748,922
Scaffold # / L50 (bp):	6 / 4,363,800	6 / 4,274,666
Contig # / L50 (bp):	6 / 4,363,800	6 / 4,274,666
Scaffold # / L90 (bp):	12 / 2,755,570	12 / 2,859,161
Contig # / L90 (bp):	16 / 545,016	15 / 739,084
Max scaffold length:	6,633,703	6,587,067
Max contig length:	6,633,703	6,587,067
% in scaffolds:	99.38%	99.14%

Table S3. Chromosome and unplaced scaffold lengths and stats for the GL1381 assembly.

Chromosome/Scaffold	Length (bp)	5' telomere?[a]	3' telomere?[a]
gl1381ChromosomeYfrag1381	2,755,570		
gl1381ChromosomeLS2	2,704,307		
gl1381ChromosomeLS3	2,212,743	TAACCC * 23	
gl1381Chromosome01	6,633,703		GGGATT * 25
gl1381Chromosome02	5,344,401		GGGATT * 20
gl1381Chromosome04	5,489,227	TAACCC * 19	GGGATT * 14
gl1381Chromosome05	5,382,151	TAACCC * 19	GGGATT * 11
gl1381Chromosome07	4,929,207		GGGATT * 23
gl1381Chromosome08	4,363,800	TAACCC * 19	
gl1381Chromosome09	3,934,070		GGGATT * 20
gl1381Chromosome10	3,411,054	TAACCC * 11	GGGATT * 11
gl1381Chromosome11	3,217,330		
gl1381Chromosome12	3,140,593	TAACCC * 15	
gl1381Chromosome13	2,952,015	TAACCC * 20	
gl1381Contig15mitochondria	40,945		
gl1381.Scaffold6	38,412		
gl1381.Scaffold9	26,869	TAACCC * 11	
gl1381.Scaffold10	31,003		
gl1381.Scaffold11	59,573		
gl1381.Scaffold13	78,826		GGGATT * 12
gl1381.Scaffold16	24,109	TAACCC * 17	
gl1381.Scaffold17	24,172		
gl1381.Scaffold19	24,287		
gl1381.Scaffold20	4,999		
gl1381.Scaffold22	35,134		
gl1381.Scaffold23	5,771	TAACCC * 19	
gl1381.Scaffold24	17,480		GGGATT * 12
gl1381.Scaffold25	4,999		
gl1381.Scaffold27	10,267		GGGATT * 11
gl1381.Scaffold28	24,661		
gl1381.Scaffold29	19,266	TAACCC * 11	
gl1381.Scaffold32	16,747		GGGATT * 22
gl1381.Scaffold33	4,999		

Total genome length (bp)	56,962,690
Length of unplaced scaffolds (bp)	451,574
% Unplaced	0.79
% Placed in biomolecules	99.21

[a] If a 5' or 3' telomeric repeat were observed, these columns indicate the repeated sequence ("TAACCC" or "GGGATT") and the number of occurrences ("* ##).

Table S4. Chromosome and unplaced scaffold lengths and stats for the GL1080 assembly.

Chromosome/Scaffold	Length (bp)	5' telomere?[a]	3' telomere?[a]
gl1080ChromosomeYfrag1080	2,964,007		GGGATT * 22
gl1080ChromosomeLS2	3,400,526		GGGATT * 18
gl1080ChromosomeLS3	1,216,525		
gl1080Chromosome01	6,587,067	TAACCC * 21	GGGATT * 11
gl1080Chromosome02	5,079,833		GGGATT * 11
gl1080Chromosome04	5,392,072	TAACCC * 21	GGGATT * 9
gl1080Chromosome05	5,277,501	TAACCC * 11	GGGATT * 23
gl1080Chromosome07	4,852,472	TAACCC * 20	GGGATT * 10
gl1080Chromosome08	4,274,666	TAACCC * 15	GGGATT * 13
gl1080Chromosome09	3,715,323	TAACCC * 9	GGGATT * 22
gl1080Chromosome10	3,249,646	TAACCC * 11	GGGATT * 18
gl1080Chromosome11	3,822,057		
gl1080Chromosome12	2,859,161		GGGATT * 22
gl1080Chromosome13	2,581,041	TAACCC * 15	GGGATT * 12
gl1080mitochondrial	45,629		
gl1080Scaffold5	13,865	TAACCC * 10	
gl1080Scaffold6	4,999		
gl1080Scaffold7	15,365	TAACCC * 17	
gl1080Scaffold8	26,188		
gl1080Scaffold10	19,919		
gl1080Scaffold11	18,831		
gl1080Scaffold12	12,125	TAACCC * 12	
gl1080Scaffold13	16,175		
gl1080Scaffold14	18,422		
gl1080Scaffold15	17,454	TAACCC * 9	
gl1080Scaffold16	18,810		
gl1080Scaffold17	38,478		
gl1080Scaffold22	35,666		
gl1080Scaffold24	18,348		
gl1080Scaffold25	11,696		
gl1080Scaffold26	8,027		
gl1080Scaffold27	22,979		
gl1080Scaffold28	17,506		
gl1080Scaffold32	21,574		
gl1080Scaffold33	28,752		
gl1080Scaffold34	24,961		
gl1080Scaffold35	8,867		
gl1080Scaffold37	14,889		

Total genome length (bp)	55,751,422	
Length of unplaced scaffolds (bp)	433,896	
% Unplaced		0.78
% Placed in biomolecules		99.22

[a] If a 5' or 3' telomeric repeat were observed, these columns indicate the repeated sequence ("TAACCC" or "GGGATT") and the number of occurrences ("* ##).

Table S5. The coverage of regions on chr$^{Y\text{-}frag}$ that are conserved among yellows-*fragariae* isolates by *F. oxysporum* Clade 2B isolates. Bedtools 'subtract' function was used to compare conserved sequences to bedfiles containing coverage coordinates by each clade 2B isolate. While no single isolate had more than 81.7% coverage, only 34,082 bp and 36,617 bp were unique to the GL1080 and GL1381 references, respectively.

	Number of basepairs on chr$^{Y\text{-}frag}$ that have coverage by the clade 2B isolate, and are conserved among yellows-*fragariae*		**The percent of sequences on chr$^{Y\text{-}frag}$ that are conserved among yellows-*fragariae* and also present in the clade 2B isolate:**	
Clade 2B isolate	**chr$^{Y\text{-}frag1381}$** (bp out of 1,366,726)	**chr$^{Y\text{-}frag1080}$** (bp out of 1,297,182)	**chr$^{Y\text{-}frag1381}$** (%)	**chr$^{Y\text{-}frag1080}$** (%)
036_niv_Fon020	1,090,274	1,059,573	79.77	81.68
034_niv_Fon010	1,079,978	1,051,054	79.02	81.03
021_niv_Fon005	1,079,937	1,048,073	79.02	80.80
033_niv_Fon013	1,054,652	1,029,424	77.17	79.36
071_lag_Lag1-1	993,257	930,473	72.67	71.73
129_fra_F74_spain	971,813	978,934	71.11	75.47
130_fra_F79_spain	964,865	971,785	70.60	74.92
086_lag_01-03008	954,900	902,963	69.87	69.61
085_lag_03-05118	917,778	893,122	67.15	68.85
070_mom_NRRL26413	765,146	733,897	55.98	56.58
083_lil_Fol39	751,816	803,783	55.01	61.96
067_mom_90NF2-1	722,034	694,260	52.83	53.52
029_cuc_Foc035	713,588	698,825	52.21	53.87
027_cuc_Foc037	712,905	676,872	52.16	52.18
117_NA_GL1551	398,492	418,385	29.16	32.25
102_NA_N-16893	379,188	390,660	27.74	30.12
137_NA_G2-4	377,807	347,958	27.64	26.82
119_NA_GL1704	357,552	385,548	26.16	29.72
106_NA_N-18842	352,622	398,451	25.80	30.72
103_NA_N-16999	326,702	340,464	23.90	26.25
120_NA_GL1702	307,162	343,992	22.47	26.52
078_nic_Ft-1512	295,453	374,025	21.62	28.83
127_mor_GL1804	269,638	350,555	19.73	27.02
118_NA_GL1552	237,544	286,242	17.38	22.07
104_fra_N-17203	222,362	299,995	16.27	23.13
134_fra_BRIP62122	219,232	309,996	16.04	23.90
131_fra_BRIP53855	219,167	309,107	16.04	23.83
132_fra_BRIP62106	213,762	307,220	15.64	23.68
100_NA_N-10226	202,028	290,650	14.78	22.41
121_NA_GL1703	195,022	257,374	14.27	19.84
136_fra_BRIP63546	194,303	172,260	14.22	13.28
099_NA_N-10010	177,018	223,154	12.95	17.20
101_NA_N-16818	157,104	250,639	11.49	19.32

Table S6. Sequencing and mapping statistics for transcriptomic experiments with GL1381. Reads were processed for quality, then mapped to the GL1381 reference genome. After mapping, reads were de-replicated based on both their position and unique molecular index (UMI) to correct for PCR duplication during library preparation.

Tissue	Timepoint	Total # of reads	# mapped reads	% of total reads mapped	# of deduplicated reads (post-UMI processing)	Reads / UMI	# of genes with at least 1 count
in planta	6 dpi	26,347,639	988,249	3.75%	268,064	3.69	8,256
in planta	6 dpi	21,967,100	501,628	2.28%	162,801	3.08	6,501
in planta	6 dpi	23,751,192	879,905	3.70%	239,415	3.68	7,344
in planta	6 dpi	25,049,361	892,078	3.56%	220,643	4.04	6,700
in planta	13 dpi	18,939,143	1,537,298	8.12%	264,126	5.82	7,371
in planta	13 dpi	19,665,888	3,483,621	17.71%	594,576	5.86	10,132
in planta	13 dpi	18,335,770	1,616,639	8.82%	385,970	4.19	9,319
in planta	13 dpi	26,020,356	912,452	3.51%	234,926	3.88	8,143
in vitro	3 dpi	6,322,460	6,080,720	96.18%	1,630,438	3.73	10,762
in vitro	3 dpi	7,610,464	7,425,112	97.56%	3,749,979	1.98	11,876
in vitro	3 dpi	17,697,528	16,854,646	95.24%	3,563,991	4.73	12,011
in vitro	3 dpi	8,026,416	7,762,634	96.71%	3,769,740	2.06	11,968

Methods S1. Pathogenicity assays with AMP132 were primarily conducted in a field at the UC Davis Plant Pathology Farm, Davis, California. The soil type was Yolo loam based on information provided by the Web Soil Survey (WSS), USDA Natural Resources Conservation Service (https://websoilsurvey.sc.egov.usda.gov/). Beds were 15.25 cm high, covered in black plastic mulch, contained a single row with 30.5 cm spacing between plants, and were arranged with 76.2 cm between bed centers. Experiments were planted in Fall 2016, Fall 2017, and Spring of 2018. Entries were arranged in a balanced square lattice design with four single-plant replications per entry. The same field was used for all experiments and had been fumigated the year prior to the first planting (Pincot *et al.*, 2018). Water was delivered via sub-surface drip irrigation as needed to maintain adequate soil moisture, and approximately 198 kg/ha of nitrogen was applied during each growing season.

Notes S1. Additional notes on symptoms caused by yellows- and wilt-*fragariae*.
The historical record supports a distinction between yellows- and wilt-*fragariae*. Chlorosis was reported as a symptom in the first reports of this disease from Japan and South Korea, and we only recovered yellows-*fragariae* isolates from these regions (Okamoto *et al.*, 1970; Kim *et al.*, 1982). In contrast, the first report of *F. oxysporum* f. sp. *fragariae* in eastern Australia (i.e. Queensland) specifically noted that chlorosis was not observed in the summer when temperatures were warm: “During the summer months, the disease causes sudden wilting of all of the leaves of the infected plant. The leaves die rapidly without showing chlorotic symptoms.” (Winks & Williams, 1965). Fortunately, we were able to test the pathogenicity of an isolate (BRIP5168) that was deposited in the Queensland Herbarium in 1965 by Barbara Winks, the author of the first report of this pathogen (Winks & Williams, 1965). This isolate likely represents the original genotype of this pathogen in eastern Australia, and it caused wilt-*fragariae* symptoms. We only recovered wilt-*fragariae* isolates from Queensland, Australia.

The daily high temperatures in our experiments, 28°C, were equivalent to average summer high temperatures in Queensland, Australia where these isolates originated. Winks and Williams (Winks & Williams, 1965) note that: “In the cooler months, the disease is less obvious, and the affected plants usually maintain a few central leaves, although these are usually rolled, chlorotic, and often stunted”. This suggests that symptom expression is influenced by temperature, but we did not test if chlorosis occurred on wilt-*fragariae*-infected plants at low temperatures. To accurately phenotype isolates of *F. oxysporum* f. sp. *fragariae*, it is essential to conduct assays with the environmental conditions described in this study.

Notes S2. A partial reconstruction of the emergence, dispersal, and diversification of *F. oxysporum* f. sp. *fragariae*.

Fusarium oxysporum was first reported as a pathogen of strawberry in eastern Australia (Queensland) in 1962 (Winks & Williams, 1965). Using an isolate deposited just three years later by the report's author, Barbara Winks, we were able to reproduce the symptoms described in this report (Additional File S1; Notes S1) (Winks & Williams, 1965). These symptoms did not include chlorosis; we called isolates with this phenotype "wilt-*fragariae*". In contrast, and consistent with the initial description of Fusarium wilt in Japan (Okamoto *et al.*, 1970), chlorosis was caused by all Japanese isolates that we tested. We called chlorosis-inducing isolates "yellows-*fragariae*". There was no overlap between wilt- and yellows-*fragariae* core genome phylogenetic groups (Fig. S4). Combined, these data strongly suggest the pathogen emerged independently in eastern Australia and Japan.

The oldest isolates we could obtain from Japan were collected at an unknown date prior to being deposited in the National Agriculture and Food Research Organization (NARO) Genebank culture collection (Fig. S4). All of their deposition dates were between 1985 and 1990, which are within 21 years after the first report of the disease in Japan (Okamoto *et al.*, 1970). However, these isolates had three distinct types of $chr^{Y\text{-}frag}$ (T1, T3, and T1381), and represented three different core genome phylogenetic groups (Y2, Y7, and Y8). This suggests that $chr^{Y\text{-}frag}$ was already polyphyletic in *F. oxysporum* in Japan and had differentiated into distinct types before the first observation of the pathogen (Fig. 4). The phylogeny of $chr^{Y\text{-}frag}$ is distinct from that of the core genome, and the different types could be the result of ancient horizontal chromosome transfer events followed by genetic drift. In addition, we observed four instances of HCT that could be much more recent. (Fig. 4).

It is possible that *Fusarium oxysporum* genotypes carrying $chr^{Y\text{-}frag}$ were introduced from Japan into South Korea with strawberry agriculture in the early 20^{th} century (Lee, 2014). Japanese strawberry plant nurseries were dispersing the pathogen on infected transplants in 1969 (Okamoto *et al.*, 1970), and the movement of plants between countries would have provided a mechanism for introduction (Nam *et al.*, 2011; Pastrana *et al.*, 2019). Alternatively, strains carrying this chromosome could have been trafficked between Japan and South Korea for centuries, given the geographic proximity and historic trade relationships between these countries. Evidence that *F. oxysporum* f. sp. *fragariae* was introduced in the early 1970's to South Korea from Japan comes from the close, core genome phylogenetic relationship between the South Korean isolate Fo80701 and late 1980's isolates from Japan: MAFF305557, MAFF305558, and MAFF712071 (Fig. S4). However, Fo80701 carries a unique $chr^{Y\text{-}frag}$ type (T2) that we did not observe in Japanese isolates of this pathogen. We did not observe any Japanese and South Korean isolates that carried the same $chr^{Y\text{-}frag}$ type. It is possible that our sampling simply did not recover isolates that are an evolutionary "link" between these countries. Alternatively, this chromosome might have arrived in South Korea and diverged into novel variants many years before the first report of the disease.

This pathogen was not documented in California until 2006 but was likely introduced from Japan and/or South Korea many years before. An extensive population survey identified three somatic compatibility groups of this pathogen in California within a few years of the first observation of this disease (Henry *et al.*, 2017). Isolates from two of these groups were also found in Japan (this study), implying multiple introductions. The third group, Y1-T1080, shares a nearly identical $chr^{Y\text{-}frag}$ type with a Y6-T1080 isolate from Korea. The emergence of this disease in California was concurrent with the phase-out of a highly effective soil fumigant, methyl bromide. Annual applications of this fumigant could have suppressed the pathogen below a threshold required for symptom expression. If symptoms were expressed, they may have been attributed to Verticillium wilt, which is a common disease in strawberry production regions. All fields where *F. oxysporum* f. sp. *fragariae* was first observed were treated by less effective fumigation practices for several preceding years (Koike & Gordon, 2015). This would have allowed buildup of pathogen populations that ultimately led to severe disease outbreaks.

Curiously, the most common genotype of *F. oxysporum* f. sp. *fragariae* in California, Y1-T1080, is also observed in Western Australia, but not in Japan or South Korea. Western Australia is geographically isolated from the original Australian populations of *F. oxysporum* f. sp. *fragariae* in Queensland. More extensive sampling of populations in Japan and South Korea is necessary to determine if this genotype (Y1-T1080) could have originated in these countries. However, it is possible that chromosome transfer to a Y1 strain in either California or Western Australia generated Y1-T1080. This genotype could have been subsequently moved on infected planting material between countries.

Compared with all other *F. oxysporum* f. sp. *fragariae* strains, the Spanish genotype that emerged between 2014 and 2016 is distinct in its host range, core genome phylogeny, and accessory genome content. These data leave little doubt of an independent origin for *F. oxysporum* f. sp. *fragariae* in Spain. Emergence of this new genotype was enabled by the widespread adoption of a new cultivar, Splendor, which is highly susceptible to this novel strain (Borrero *et al.*, 2017). Other cultivars (such as ‘Sweet Ann’ or ‘Camarosa’) that are susceptible to all other *F. oxysporum* f. sp. *fragariae* strains are resistant to the Spanish genotype. This illustrates how host diversity can generate pathogen diversity; the strain would not have been recovered and characterized as *F. oxysporum* f. sp. *fragariae* if strawberry production in Spain continued with cultivar Camarosa.

Additional File S1 (separate file). Isolate metadata. Isolate IDs, source information, amplification with PCR diagnostic loci, and GenBank accessions are provided in this table.

Additional File S2 (separate file). Genome metadata. This spreadsheet contains annotation and assembly stats, GenBank Assembly and SRA accessions, and clade designations for all genomes compared in this study.

Additional File S3 (separate file). Raw scores for Fusarium wilt resistance phenotypes at final timepoints for all experiments. Includes all of *Fragaria* spp. accessions x isolate combinations tested in this study.

Additional File S4 (separate file). A '.bed' formatted file with the coordinates of sequences in the GL1381 genome that are conserved among all 27 yellows-fragariae isolates tested.

Additional File S5 (separate file). A '.bed' formatted file with the coordinates of sequences in the GL1080 genome that are conserved among all 27 yellows-fragariae isolates tested.

Additional File S6 (separate file). Genes differentially expressed on $chr^{Yfrag1381}$ and lineage specific chromosomes at 6- and 13-days post-inoculation *in planta* vs. *in vitro*. The position of these genes and their SignalP and EffectorP predictions are included.

Additional File S7 (separate file). Genotype matrix for all *Fragaria* spp. analyzed in this study. Genotype calls on an 50k SNP octoploid strawberry array for all *Fragaria* spp. genotypes we tested for resistance to *F. oxysporum* f. sp. *fragariae*.

Additional File S8 (separate file). Metadata and least-squares means for all *Fragaria* spp. x isolate combinations tested in the differential resistance panel. For each *Fragaria* spp. accession tested, the year and location of origin, common name, and U.S. Plant Germplasm Identifier are provided. Where possible, citations about the origin of the cultivar are included.

SI References

Borrero C, Bascon J, Gallardo MA, Orta MS, Aviles M. 2017. New foci of strawberry Fusarium wilt in Huelva (Spain) and susceptibility of the most commonly used cultivars. *Scientia Horticulturae* **226**: 85-90.

Henry PM, Kirkpatrick SC, Islas CM, Pastrana AM, Yoshisato JA, Koike ST, Daugovish O, Gordon TR. 2017. The population of *Fusarium oxysporum* f. sp. *fragariae*, cause of Fusarium wilt of strawberry, in California. *Plant Disease* **101**: 550-556.

Kim CH, Seo HD, Cho WD, Kim SB. 1982. Studies on varietal resistance and chemical control to the wilt of strawberry caused by *Fusarium oxysporum*. *Korean Journal of Plant Protection* **21**: 61-67.

Koike ST, Gordon TR. 2015. Management of Fusarium wilt of strawberry. *Crop Protection* **73**: 67-72.

Lee WS. 2014. Production of ever-bearing strawberry and production technology in Korea. *Acta horticulturae* **1049**: 561-564.

Nam MH, Kang YJ, Lee IH, Kim HG, Chun C. 2011. Infection of daughter plants by *Fusarium oxysporum* f. sp. *fragariae* through runner propagation of strawberry. *Korean Journal of Horticultural Science and Technology* **29**: 273-277.

Okamoto H, Fujii S, Kato K, Yoshioka A. 1970. A new strawberry disease 'Fusarium wilt'. *Plant Protection* **24**: 231-235.

Pastrana AM, Watson DC, Gordon TR. 2019. Transmission of *Fusarium oxysporum* f. sp. *fragariae* through stolons in strawberry plants. *Plant Disease* **103**: 1249-1251.

Pincot DDA, Poorten TJ, Hardigan MA, Harshman JM, Acharya CB, Cole GS, Gordon TR, Stueven M, Edger PP, Knapp S. 2018. Genome-wide association mapping uncovers *Fw1*, a dominant gene conferring resistance to Fusarium wilt in strawberry. *G3: Genes, Genomes, Genetics* **8**: 1817-1828.

Winks BL, Williams YN. 1965. A wilt of strawberry caused by a new form of *Fusarium oxysporum*. *Queensland Journal of Agricultural and Animal Science* **22**: 475-479.